Title

Genetic Correction of Induced Pluripotent Stem Cells From a Deaf Patient With MYO7A Mutation Results in Morphologic and Functional Recovery of the Derived Hair Cell-Like Cells.

Journal

Stem cells translational medicine, 5(5)

ISSN

2157-6564

Authors

Tang, Zi-Hua
Chen, Jia-Rong
Zheng, Jing
et al.

Publication Date

2016-05-01

DOI

10.5966/sctm.2015-0252

STEM CELLS TRANSLATIONAL MEDICINE®

PLURIPOTENT STEM CELLS

Genetic Correction of Induced Pluripotent Stem Cells From a Deaf Patient With *MYO7A* Mutation Results in Morphologic and Functional Recovery of the Derived Hair Cell-Like Cells

ZI-HUA TANG,[a] JIA-RONG CHEN,[a] JING ZHENG,[b] HAO-SONG SHI,[c] JIE DING,[a] XIAO-DAN QIAN,[d] CUI ZHANG,[a] JIAN-LING CHEN,[a] CUI-CUI WANG,[a] LIANG LI,[a] JUN-ZHEN CHEN,[e] SHAN-KAI YIN,[c] TAO-SHENG HUANG,[f] PING CHEN,[g] MIN-XIN GUAN,[b] JIN-FU WANG[a]

[a]Institute of Cell and Development, College of Life Sciences, [b]Institute of Genetics, School of Medicine, and [d]The Affiliated Women's Hospital, Zhejiang University, Hangzhou, Zhejiang, People's Republic of China; [c]Department of Otorhinolaryngology, Shanghai Jiao Tong University Affiliated Sixth People's Hospital Shanghai, People's Republic of China; [e]Department of Otolaryngology, The Affiliated Wenling People's Hospital, Wenzhou Medical University, Wenling, Zhejiang, People's Republic of China; [f]Division of Human Genetics, Cincinnati Children's Hospital Medical Center, Cincinnati, Ohio, USA; [g]Departments of Cell Biology and Otolaryngology, Emory University School of Medicine, Atlanta, Georgia, USA

Correspondence: Jin-Fu Wang, Ph.D., Institute of Cell and Development, College of Life Sciences, Zi-Jin-Gang Campus of Zhejiang University, No. 866, Yuhangtang Road, Hangzhou, Zhejiang 310058, People's Republic of China. Telephone: 86-571-8820-6592; E-Mail: wjfu@zju.edu.cn.

Received September 16, 2015; accepted for publication December 22, 2015; published Online First on March 24, 2016.

1066-5099/2016/$20.00/0

http://dx.doi.org/10.5966/sctm.2015-0252

Key Words. Human induced pluripotent stem cells • *MYO7A* • Deafness • Genetic correction • Inner ear hair cells • Rescue

ABSTRACT

The genetic correction of induced pluripotent stem cells (iPSCs) induced from somatic cells of patients with sensorineural hearing loss (caused by hereditary factors) is a promising method for its treatment. The correction of gene mutations in iPSCs could restore the normal function of cells and provide a rich source of cells for transplantation. In the present study, iPSCs were generated from a deaf patient with compound heterozygous *MYO7A* mutations (c.1184G>A and c.4118C>T; P-iPSCs), the asymptomatic father of the patient (*MYO7A* c.1184G>A mutation; CF-iPSCs), and a normal donor (*MYO7A*$^{WT/WT}$; C-iPSCs). One of *MYO7A* mutation sites (c.4118C>T) in the P-iPSCs was corrected using CRISPR/Cas9. The corrected iPSCs (CP-iPSCs) retained cell pluripotency and normal karyotypes. Hair cell-like cells induced from CP-iPSCs showed restored organization of stereocilia-like protrusions; moreover, the electrophysiological function of these cells was similar to that of cells induced from C-iPSCs and CF-iPSCs. These results might facilitate the development of iPSC-based gene therapy for genetic disorders.

STEM CELLS TRANSLATIONAL MEDICINE *2016;5:561–571*

SIGNIFICANCE

Induced pluripotent stem cells (iPSCs) were generated from a deaf patient with compound heterozygous *MYO7A* mutations (c.1184G>A and c.4118C>T). One of the *MYO7A* mutation sites (c.4118C>T) in the iPSCs was corrected using CRISPR/Cas9. The genetic correction of *MYO7A* mutation resulted in morphologic and functional recovery of hair cell-like cells derived from iPSCs. These findings confirm the hypothesis that MYO7A plays an important role in the assembly of stereocilia into stereociliary bundles. Thus, the present study might provide further insight into the pathogenesis of sensorineural hearing loss and facilitate the development of therapeutic strategies against monogenic disease through the genetic repair of patient-specific iPSCs.

INTRODUCTION

Artificial cochlear implants are effective corrective measures for sensorineural hearing loss. However, long-term strategies such as stem cell treatment are required for successful and comprehensive treatment of this disease. Recent studies have focused on inducing the differentiation of several types of human stem cells into hair cell-like cells in vitro. Recent studies have reported the induction of human embryonic stem cell (ESC) differentiation into inner ear hair cell-like cells [1, 2]. However, the restricted availability, potential immunorejection after allogenic cell transplantation, and rare derivation of cell lines with the same gene mutation pattern could restrict the treatment of hereditary hearing loss. Induced pluripotent stem cells (iPSCs), which are highly similar to ESCs, are derived from human adult somatic tissues, such as human skin fibroblasts [3], urinary cells [4], and lymphocytes [5, 6]. Human iPSCs have been generated from patients with amyotrophic lateral sclerosis [7], spinal muscular atrophy [8], cardiomyopathy [9], and diabetes [10]. These disease-specific iPSCs can be induced to differentiate into disease-relevant cells, and the genetic correction of disease-specific genes in iPSCs increases the feasibility of the disease's treatment using stem cells.

MYO7A mutations in patients with hereditary deafness are associated with profound congenital neurosensory nonsyndromal deafness (DFNB2; DFNA11) and Usher syndrome type 1B (USH1B) [11, 12]. MYO7A is an unconventional myosin expressed only in the cytoplasm and stereocilia of inner and outer hair cells of the cochlea [13], which contains three domains: the highly conserved motor domain, a neck region (five IQ motifs), and a tail region containing two MyTH4-FERM domains separated by an SH3 domain. Previous studies have theorized that MYO7A might have an important role in assembling the stereocilia into a bundle, maintaining the rigidity of the bundle [14], and controlling the actin dynamics within the stereocilia [15], thereby maintaining a normal functionality of the hair cells. In our previous study, deafness in a 7-year-old girl was attributed to compound heterozygous *MYO7A* mutations (c.1184G>A and c.4118C>T), and her asymptomatic parents expressed only one heterozygous *MYO7A* mutation each. Therefore, we attempted to generate iPSCs from the urinary cells of the patient. Next, one *MYO7A* mutation locus (c.4118C>T) in the iPSCs induced from the patient was genetically corrected using the CRISPR-Cas9 system to establish a new iPSC line. The iPSCs were induced to differentiate into hair cell-like cells, and the effects of genetic correction of the *MYO7A* mutations on the characteristics and recovery function of the hair cell-like cells were analyzed and are discussed.

Materials and Methods

Cells and Culture

The Zhejiang Health Bureau and Institutional Ethics Committee of the First People Hospital of Wenling approved the urine sample collection. iPSCs were generated from the urinary cells of the deaf patient with compound heterozygous *MYO7A* c.1184G>A and c.4118C>T mutations (P-iPSCs), the patient's asymptomatic father with a *MYO7A* c.1184G>A mutation (CF-iPSCs), and a healthy donor with normal $MYO7A^{WT/WT}$ (C-iPSCs). All donors provided informed consent before sample collection. The Zhejiang University Institutional Stem Cell Research Oversight Committee approved the laboratory research on the derivation and use of human iPSC lines in accordance with local regulations. All procedures involving animals were conducted in compliance with guidelines established by the Zhejiang University Institutional Animal Care and Use Committee. Details and culture procedures, including hair cell differentiation [1], are provided in the supplemental online data.

CRISPR-Cas9-Mediated Gene Correction of *MYO7A* Mutation (c. 4118C>T) in P-iPSCs

An enhanced green fluorescent protein (maxGFP)-expressing pX330 vector was generated by linking the *Not*I digested maxGFP amplicons and pX330 vector using the T4 DNA ligase. The target sequence for the *MYO7A* gene was synthesized using the CRISPR Design Tool (available at http://tools.genome-engineering.org/); a single maxGFP-Cas9-sgRNA expressing vector was finally generated by phosphorylating, annealing, and inserting two oligos into the GFP-expressing pX330 vector, using the *Bbs*I restriction enzyme site. The maxGFP-Cas9-sgRNA vector was functionally validated in 293T cells. A P-iPSC cell suspension was transfected with the hCas9 expression vector and single strand oligodeoxynucleotide and transferred to human ESC medium. The cell mass derived from each single cell was cultured to derive genetically corrected clones. These clones were confirmed by sequencing and restriction enzyme analysis. The cas9 cleavage efficiency was assessed by Sanger sequencing. Potential off-target sites were selected using the CRISPR Design Tool (available at http://tools.genome-engineering.org/), and the amplicons were sequenced and analyzed using nucleotide basic local alignment search tool (National Center for Biotechnology Information). Further details of the methods (primers, restriction enzyme analysis, vector generation) used are provided in the supplemental online data.

RNA Isolation and Gene Expression Analysis

Total RNA was isolated and reverse transcribed to cDNA, which was used as the template for PCR. The primer sequences are provided in the supplemental online data.

Immunocytochemistry

Cells cultured on cover slips were fixed, permeabilized, and processed for immunocytochemistry with antibodies, as detailed in the supplemental online data. Images were obtained using a Zeiss confocal microscope. For conventional quantification, several hundred cells from three to five independent experiments were scored from random fields. Cells at the threshold of fluorescence intensity were counted as positive. The threshold was set according to the fluorescent intensity distribution histogram of cells in the control (no primary antibody) wells. The cells were counted as positive, green, or red, if the fluorescent intensity was greater than the 99th intensity percentile point in channel 2 (green) or 3 (red), respectively.

Western Blot Analysis

Total protein was extracted from 3-week differentiated hair cell-like cells using RIPA lysis buffer and processed for Western blot analysis. The details of this procedure are provided in the supplemental online data.

Scanning Electron Microscopy

Cells growing on cover slips were fixed sequentially with 2.5% glutaraldehyde and osmic acid, dehydrated with a sequential dilution of ethanol, treated with isoamyl acetate, and observed on a metal conductive column after plating (the samples) with gold. The scanning electron microscopy samples were prepared as detailed in the supplemental online data.

Electrophysiology

The membrane currents of cells cultured for 3 to 4 weeks under hair cell differentiation conditions were measured using the whole-cell patch-clamp technique with the aid of an amplifier (EPC 10; HEKA Electronik). Voltage protocol application and data acquisition were performed using Pulse software, version 6.0 (HEKA Electronik). Details of the measurement procedure are provided in the supplemental online data.

Statistical Analysis

All data are presented as the mean ± SD of the independent experiments. The mean values were statistically compared using an unpaired Student's two-tailed *t* test for two data sets; *p* values $<.05$ were considered statistically significant.

RESULTS

Generation and Characterization of iPSCs Induced From Human Urinary Cells

Information collected from the family of the deaf patient via genetic analyses is shown in supplemental online Figure 1. Her parents were asymptomatic with normal hearing (supplemental online Fig. 1A, 1C). In contrast, the auditory threshold of the patient was much higher in the low frequency sound wave section and increased rapidly in the high frequency section (supplemental online Fig. 1D). The patient finally lost her hearing in the higher frequency section. The *MYO7A* gene of the patient contained heterozygous double mutations (c.1184G>A and c.4118C>T; acquired from each parent), and the father and mother were each heterozygous for the *MYO7A* c.1184G>A and *MYO7A* c.4118C>T mutation, respectively (supplemental online Fig. 1B).

Three iPSC lines (P-iPSCs, CF-iPSCs, and C-iPSCs) were generated from the urinary cells (supplemental online Fig. 2A) of the patient, her asymptomatic father, and a healthy donor (female, age 26 years), respectively, by retroviral infection of four reprogramming factors: Oct4, Sox2, c-Myc, and Klf4. All iPSCs exhibited the morphological characteristics of human ESCs (Fig. 1A). They stained positively for alkaline phosphatase (supplemental online Fig. 2B), expressed the pluripotent markers NANOG, OCT4, Tra-I-60, Tra-I-81, and SSEA-4 (Fig. 1C), and maintained a stable karyotype (supplemental online Fig. 2C). Reverse transcription polymerase chain reaction (PCR) analysis revealed that all three iPSC lines expressed endogenous pluripotent genes (*OCT4*, *NANOG,* and *SOX2*; supplemental online Fig. 2D). The subcutaneous injection of these iPSCs into immunodeficient severe combined immunodeficiency mice resulted in the formation of teratomas containing advanced tissue derivatives of all three germ layers (Fig. 1B). The results of sequencing of the *MYO7A* gene from the P-iPSCs and CF-iPSCs were in accordance with the previous identification of their blood genetics (supplemental online Fig. 2E).

Differentiation of iPSCs Into Otic Progenitors and Inner Ear Hair Cell-Like Cells

iPSCs were subjected to otic differentiation (supplemental online data). After 12 days of differentiation, all three iPSCs were induced into two cell types with different morphologies: otic epithelial progenitors (OEPs) and otic neural progenitors (ONP) (Fig. 2A). OEPs are inclined to differentiate into hair cell-like cells under "hair cell" culture conditions [1]. The differentiation of otic progenitors was defined by immunostaining with antibodies specific for PAX2 [16], PAX8 [17], and SOX2 [18] (Fig. 2B, 2C). The results revealed that cells derived from C-iPSCs, P-iPSCs, and CF-iPSCs contained 58.6% $\pm$ 9.1% (n = 5), 50.2% $\pm$ 11.8% (n = 5), and 47.6% $\pm$ 11.1% (n = 5) PAX2-PAX8 double-positive cells, respectively (Fig. 2D) and 73.3% $\pm$ 10.8% (n = 5), 60.3% $\pm$ 10.3% (n = 5), and 67.5% $\pm$ 7.6% (n = 5) cells coexpressing PAX8 and SOX2, respectively (Fig. 2E). Reverse transcription-PCR also demonstrated the abundant expression of several genes specifically expressed during early otic development (supplemental online Fig. 3B, 3C), such as *SOX2*, *GATA3*, *PAX2*, *PAX8*, *DLX5*, *SIX1*, and *EYA1* [17, 19–23]. The absence of the hair cell marker *ATOH1* [24, 25] indicated that hair cell differentiation had not been initiated (supplemental online Fig. 3B, 3C). These results revealed that all three iPSCs could potentially differentiate into otic progenitors.

OEPs separated from otic progenitors were induced to differentiate into hair cell-like cells on mitotically inactivated chicken utricle stromal cells. Cells derived from C-iPSCs, P-iPSCs, and CF-iPSCs all showed simultaneous ATOH1-POU4F3 (Fig. 3A) and POU4F3-MYO7A (Fig. 3B) expression. Very small percentages of cells derived from C-iPSCs (10.5% $\pm$ 4.7% [n = 5]), P-iPSCs (9.4% $\pm$ 2.6% [n = 5]), and CF-iPSCs (7.7% $\pm$ 2.9% [n = 5]) were double immunolabeled with POU4F3 and Espin (Fig. 3C; supplemental online Fig. 3A). Gene expression analysis revealed that cells induced from iPSCs expressed the hair cell markers *MYO7A*, *ATOH1*, *POU4F3*, *CHRNA9*, and *ESPN* [26–29] (supplemental online Fig. 3D, 3E). Therefore, these results showed that all iPSC-derived OEPs could differentiate into hair cell-like cells.

A major morphological characteristic of inner ear hair cells is the stereocilia-like protrusion structure. F-actin and MYO7A double-labeled stereocilia-like protrusions from hair cell-like cells derived from three iPSCs were observed by immunofluorescence (Fig. 4A); these protrusions were confirmed by scanning electron microscopy (Fig. 4B). However, the stereocilia-like protrusions from the three iPSCs showed some differences. The stereocilia-like protrusions of hair cell-like cells differentiated from C- and CF-iPSCs appeared to be hard and straight, with some stuck together. The stereocilia-like protrusions of the hair cell-like cells differentiated from P-iPSCs were curving, disheveled, and scattered and exhibited no bonding with each other. MYO7A expression was examined in cells differentiated from C-, CF-, and P-iPSCs. Immunoblotting with an antibody specific for both normal and mutant MYO7A revealed that hair cell-like cells derived from P-iPSCs expressed an extra protein with a molecular weight ranging from 140 to 250 kDa compared with hair cell-like cells derived from C- and CF-iPSCs (Fig. 4C).

The functional activity of mechanotransduction (MET) channels in hair cell-like cells was determined by incubating the cells differentiated from C-, CF-, and P-iPSCs with FM1-43FX. Hair cell-like cells derived from the three iPSCs showed rapid uptake of the FM1-43 dye (Fig. 5A). However, the hair cell-like cells differentiated from P-iPSCs taking up the FM1-43 dye were much fewer than those differentiated from C-iPSCs and CF-iPSCs. In addition, the hair cell-like cells stained with FM1-43 showed electrophysiological recordings of a voltage-dependent outward K^+ current, an inward rectifier K^+ current (I_{K1}), and an inward Ca^{2+} current (I_{Ca}) (Fig. 5B–5D), which revealed the specific electrophysiological activities of the hair cells. However, the I_{K1}, and I_{Ca} recorded in hair cell-like cells derived from P-iPSCs were significantly higher than that in hair cell-like cells derived from the C- and CF-iPSCs (Fig. 5F, 5G).

Effects of CRISPR-Cas9-Mediated Gene Correction on Morphology and Function Recovery of Hair Cell-Like Cells Induced From P-iPSCs

We tried to correct the *MYO7A* c.4118C>T mutation in the P-iPSC line using the CRISPR/Cas9 system and to examine the effects of genetic correction on the morphology and function recovery of induced hair cell-like cells. Three guide-RNA sequences adjacent to the targeting site were cloned into the maxGFP-expressing pX330 (supplemental online Fig. 4A; supplemental online Table 1). gRNA1 was selected for all

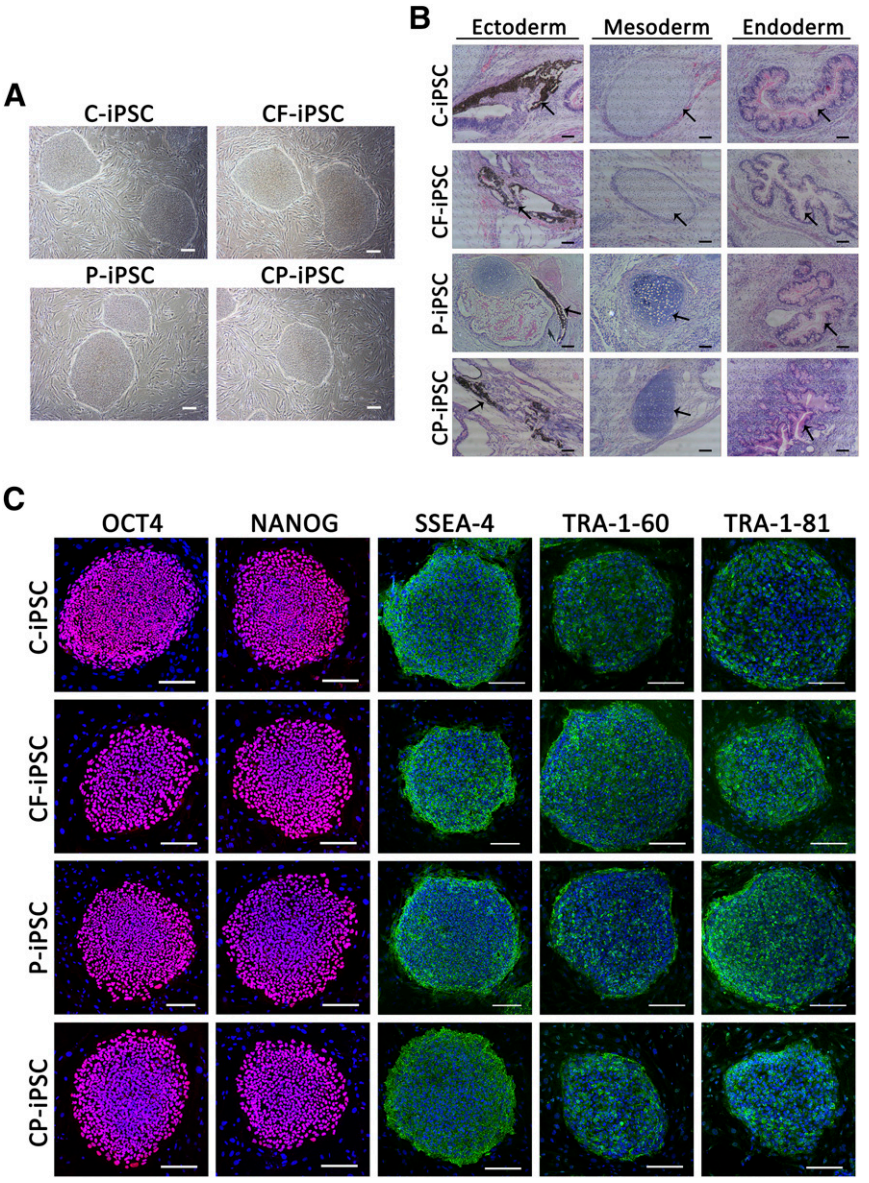

Figure 1. Morphological and pluripotency characteristics of P-iPSCs, CF-iPSCs, C-iPSCs, and CP-iPSCs. **(A):** Morphology of iPSCs derived from the normal donor (C-iPSCs), patient (P-iPSCs), asymptomatic father (CF-iPSCs), and genetically corrected iPSCs (CP-iPSCs). Scale bars = 200 μm. **(B):** Hematoxylin and eosin staining of teratomas derived from iPSCs, showing a pigmented epithelium (ectoderm), gastrointestinal epithelium (endoderm), and hyaline cartilage (mesoderm). Scale bars = 100 μm. **(C):** Immunostaining of C-iPSCs, P-iPSCs, CF-iPSCs, and CP-iPSCs with antibodies specific for the pluripotency markers: OCT4, NANOG, SSEA-4, TRA-1-60, and TRA1-81. Nuclei were stained with 4′,6-diamidino-2-phenylindole (blue). Scale bars = 200 μm. Abbreviations: C-iPSCs, control induced pluripotent stem cells; CF-iPSCs, induced pluripotent stem cells from the asymptomatic father of the patient (*MYO7A* c.1184G>A mutation); CP-iPSCs, genetically corrected induced pluripotent stem cells; iPSCs, induced pluripotent stem cells; P-iPSCs, induced pluripotent stem cells derived from deaf patient with compound heterozygous *MYO7A* mutations (c.1184G>A and c.4118C>T).

subsequent experiments because of its relatively higher disorder peak rate and because its cutting site was only 8-base pair (bp) from the site to be corrected. P-iPSCs were then transfected with maxGFP-pX330 and the HDR template (150-bp single strand oligodeoxynucleotide) by electrotransfection (transfection efficiency, 11%; detected by fluorescence-activated cell sorting; supplemental online Fig. 5). After the GFP-expressing cells sorted by fluorescence-activated cell sorting were expanded, 45 clones were picked, processed by genomic PCR, and sequenced to verify the gene correction. Finally, three clones (designated as CP-iPSCs1, CP-iPSCs2, and CP-iPSCs3) were repaired; the representative sequencing results are shown in supplemental online Figure 4B. The restriction endonuclease *BstAP*I was used to verify the gene correction (supplemental online Fig. 4D). The wild-type sequence was cleaved by *BstAP*I; however, the mutant sequence could not be cleaved by this enzyme. Therefore, the 584-bp PCR amplicon containing the targeting site in the C- and CP-iPSCs could be thoroughly cleaved into two fragments (197 and 387 bp). However, only the normal chromosome-derived amplicons could be cut off from the P-iPSCs; therefore, the enzyme-digested product contained three fragments (197 bp, 387 bp, and 584 bp). The amplicons of the three CP-iPSC lines

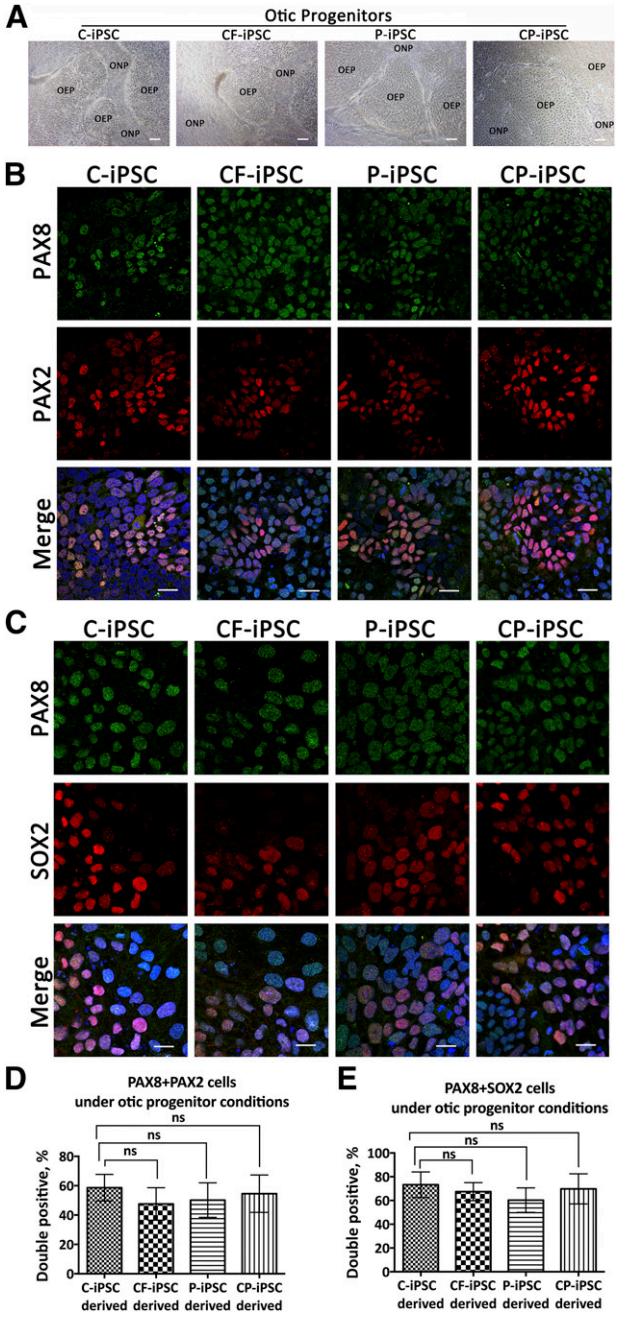

Figure 2. Differentiation into otic progenitor cells. **(A):** Morphology of otic epithelial progenitor and otic neural progenitor colonies derived from C-iPSCs, CF-iPSCs, P-iPSCs, and CP-iPSCs. Scale bars = 200 μm. **(B):** Coexpression of otic markers PAX2 and PAX8 in otic progenitors derived from C-iPSCs, CF-iPSCs, P-iPSCs, and CP-iPSCs. Scale bars = 20 μm. **(C):** Coexpression of otic markers PAX8 and SOX2 in otic progenitors derived from C-iPSCs, CF-iPSCs, P-iPSCs, and CP-iPSCs. Scale bars = 20 μm. **(D):** Percentage of PAX8/PAX2 double-positive cells in the total cell population. Error bars represent the SD (n = 5). **(E):** Coexpression of otic markers PAX8 and SOX2 in otic progenitors derived from C-iPSCs, CF-iPSCs, P-iPSCs, and CP-iPSCs. Error bars represent the SD (n = 5). Abbreviations: C-iPSCs, control induced pluripotent stem cells; CF-iPSCs, induced pluripotent stem cells from the asymptomatic father of the patient (*MYO7A* c.1184G>A mutation); CP-iPSCs, genetically corrected induced pluripotent stem cells; iPSCs, induced pluripotent stem cells; ns, not significant; OEP, otic epithelial progenitor; ONP, otic neural progenitors; P-iPSCs, induced pluripotent stem cells from the deaf patient with compound heterozygous *MYO7A* mutations (c.1184G>A and c.4118C>T).

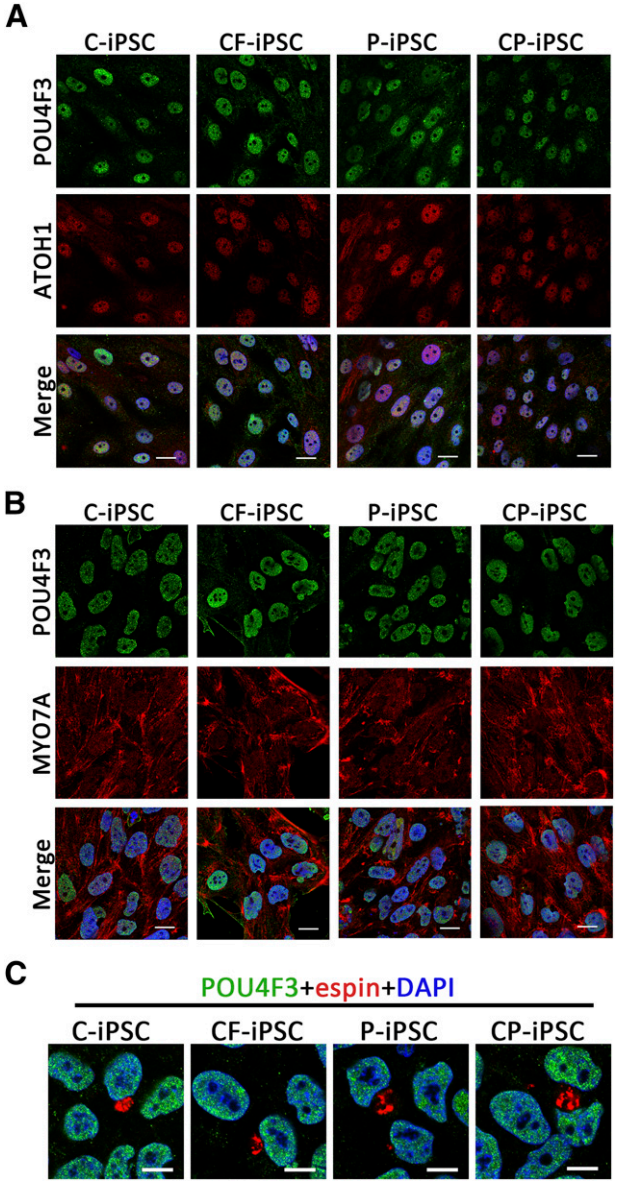

Figure 3. Differentiation of otic epithelial progenitors into hair cell-like cells. **(A):** Coexpression of otic markers POU4F3 and ATOH1 in hair cell-like cells induced from C-iPSCs, CF-iPSCs, P-iPSCs, and CP-iPSCs. Scale bars = 20 μm. **(B):** Coexpression of otic markers POU4F3 and MYO7A in hair cell-like cells induced from C-iPSCs, CF-iPSCs, P-iPSCs, and CP-iPSCs. Scale bars = 20 μm. **(C):** Coexpression of otic markers POU4F3 and Espin in hair cell-like cells induced from C-iPSCs, CF-iPSCs, P-iPSCs, and CP-iPSCs. Scale bars = 10 μm. Abbreviations: C-iPSCs, control induced pluripotent stem cells; CF-iPSCs, induced pluripotent stem cells from the asymptomatic father of the patient (*MYO7A* c.1184G>A mutation); CP-iPSCs, genetically corrected induced pluripotent stem cells; DAPI, 4′,6-diamidino-2-phenylindole; iPSCs, induced pluripotent stem cells; P-iPSCs, induced pluripotent stem cells from deaf patient with compound heterozygous *MYO7A* mutations (c.1184G>A and c.4118C>T).

containing the other mutation site (c.1184G>A) were also sequenced (supplemental online Fig. 4C). The double peaks (G and A) of the mutation site indicated the existence of this heterozygous mutation; this showed that CP-iPSCs were derived from gene targeting, rather than from C-iPSCs. The possible off-targeting efficiency of Cas9 was monitored by analyzing the

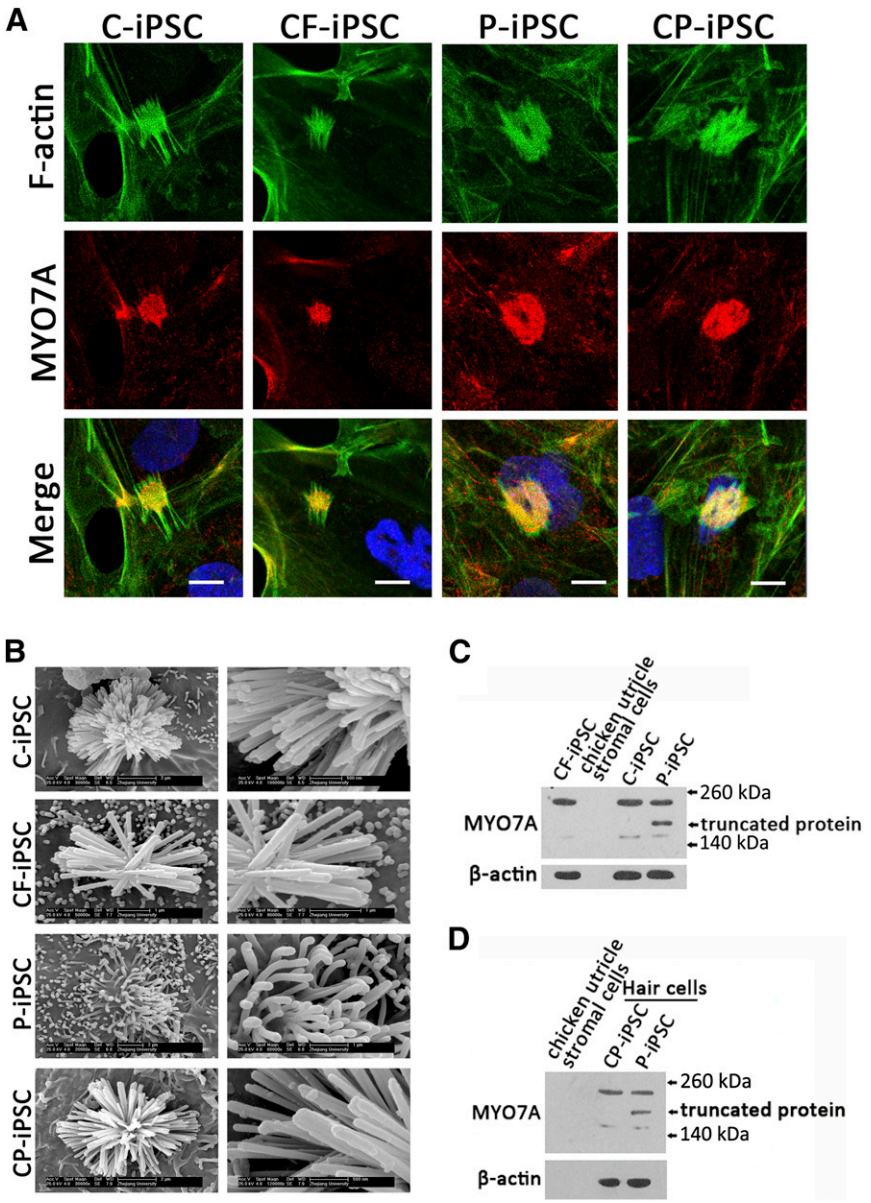

Figure 4. Hair bundle-like structures and Western blotting for MYO7A protein in cells induced from iPSCs. **(A):** Hair bundle-like protrusions in cells induced from C-iPSCs, CF-iPSCs, P-iPSCs, and CP-iPSCs, as observed by laser scanning confocal microscopy. F-actin-filled membrane protrusions were detected by staining with fluorescein isothiocyanate-conjugated phalloidin (green). The actin-bundling protein MYO7A was detected by staining with Alexa-conjugated secondary antibodies (red). Scale bars = 10 μm. **(B):** Scanning electron microscopy views of the surface of hair cell-like cells induced from C-iPSCs, CF-iPSCs, P-iPSCs, and CP-iPSCs after 3 weeks of culture on mitotically inactivated chicken utricle stromal cells. For the stereocilia-like protrusions derived from C-iPSCs and CP-iPSCs, scale bars = 2 μm (left) and 500 nm (right); for the stereocilia-like protrusions derived from CF-iPSCs, scale bar = 1 μm; for the stereocilia-like protrusions derived from P-iPSCs, scale bars = 2 μm (left) and 1 μm (right). **(C, D):** Western blotting for MYO7A protein in hair cell-like cells induced from C-iPSCs, CF-iPSCs, P-iPSCs, and CP-iPSCs. Total protein was extracted from hair cell-like cells induced from C-iPSCs, CF-iPSCs, P-iPSCs, CP-iPSCs, and mitotically inactivated chicken utricle stromal cells. β-Actin was used as the internal reference. Protein truncation had disappeared in hair cell-like cells induced from CP-iPSCs. Abbreviations: C-iPSC, control induced pluripotent stem cells; CF-iPSC, induced pluripotent stem cells from the asymptomatic father of the patient (*MYO7A* c.1184G>A mutation); CP-iPSC, genetically corrected induced pluripotent stem cells; P-iPSC, induced pluripotent stem cells from deaf patient with compound heterozygous *MYO7A* mutations (c.1184G>A and c.4118C>T).

top seven and three potential off-targeting sites outside and within the exon, respectively. No change was detected in the obtained sequences using primers (supplemental online Table 2) coding for the relevant sites compared with the sequences extracted from the National Center for Biotechnology Information. Therefore, off-targeting was not detected at these sites in the CP-iPSCs. The cas9 cleavage or HDR-mediated target modification efficiency was assessed by isolating the genomic DNA of P-iPSCs 3 days after nuclease transfection and analyzing these by Sanger sequencing of the amplicons. We observed the presence of 8.3% insertions and 29.2% deletions (supplemental online Fig. 6).

One CP-iPSC line was randomly selected for subsequent analyses. This line retained the pluripotency of iPSCs, as shown

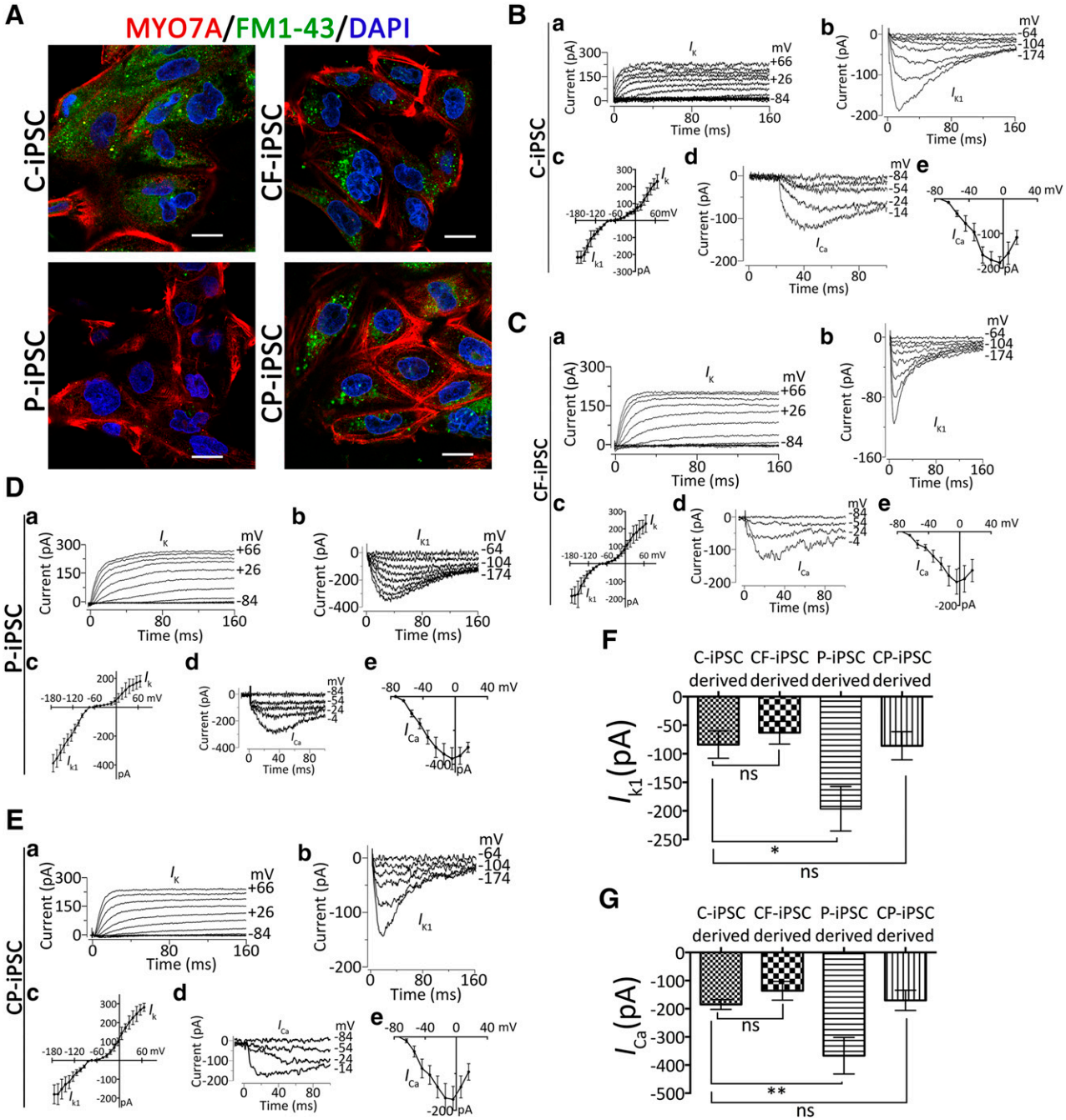

Figure 5. Physiological activity of hair cell-like cells induced from four iPSCs. **(A):** Double labeling of FM1-43FX (green) and MYO7A (red) in hair cell-like cells induced from C-iPSCs, CF-iPSCs, P-iPSCs, and CP-iPSCs. Scale bars = 20 μm. **(B–E):** Electrophysiological properties of hair cell-like cells induced from C-, CF-, P-, and CP-iPSCs. **(Ba, Bb, Ca, Cb, Da, Db, Ea, Eb):** Outward and inward K^+ currents recorded from the induced hair cell-like cells. Currents were elicited by 10 voltage steps from the holding potential (**[a]** subpanels, −84 mV; **[b]** subpanels, −64 mV). The outward K^+ current was recorded from 9 of 12, 10 of 13, 7 of 11, and 7 of 10 hair cell-like cells induced from C-, CF-, P-, and CP-iPSCs, respectively. **(Bc, Cc, Dc, Ec):** Average current-voltage (I-V) curve for outward and inward K^+ current measured at the steady-state level (160 ms). I_K at 6 mV: 76.67 ± 20.6 pA (n = 8, C-iPSC); 109 ± 25 pA (n = 6, CF-iPSC); 65 ± 30 pA (n = 7, P-iPSC); 143 ± 33 pA (n = 7, CP-iPSC). I_{K1} at −124 mV: −84.0 ± 23.9 pA (n = 8, C-iPSC); −63 ± 20 pA (n = 6, CF-iPSC); −196.3 ± 39 pA (n = 7, P-iPSC); and −86 ± 24.6 pA (n = 7, CP-iPSC). The inward and outward I_K and I_{K1} closely resembled those recorded in pre-hearing mouse cochlear hair cells [57], hair cell-like cells differentiated from human fetal auditory stem cells [58], and human embryonic stem cells [1]. **(Bd, Cd, Dd, Ed):** Example of inward Ca^{2+} current (I_{Ca}) produced by hair cell-like cells. I_{Ca} was observed in 8 of 12, 6 of 10, 6 of 11, and 6 of 10 hair cell-like cells induced from C-, CF-, P-, and CP-iPSCs, respectively. **(Be, Ce, De, Ee):** Average I-V curve for I_{Ca}. Peak I_{Ca}: −184.7 ± 17.7 pA (n = 8, C-iPSC); −136 ± 33.3 pA (n = 6, CF-iPSC); −366.7 ± 65.1 pA (n = 6, P-iPSC); and −170.2 ± 35.8 pA (n = 6, CP-iPSC). The hyperpolarized activation range of I_{Ca} indicated the presence of an L-type Ca^{2+} channel containing the CaV1.3 subunit [59], as previously seen in mammalian cochlear inner hair cells [60]. **(F):** I_{K1} measured at −124 mV as a function of cell differentiation. **(G):** I_{Ca} measured at −4 mV as a function of cell differentiation. Values plotted as the mean ± SD. Abbreviations: C-iPSCs, control induced pluripotent stem cells; CF-iPSCs, induced pluripotent stem cells from the asymptomatic father of the patient (*MYO7A* c.1184G>A

(*Figure legend continues on next page*.)

by the expression of the OCT4, SOX2, SSEA-4, TRA-1-60, and TRA-1-81 markers (Fig. 1C), maintained normal karyotypes (supplemental online Fig. 2C), and formed teratomas containing three germ layers in vivo (Fig. 1B). These results demonstrated that CP-iPSCs maintained their pluripotency. Furthermore, we confirmed that genetic correction by CRISPR restored the *MYO7A* gene products by inducing CP-iPSC differentiation into hair cell-like cells. CP-iPSCs were first induced to differentiate into otic progenitors. Immunostaining illustrated that differentiated cells were double labeled with PAX2-PAX8 (Fig. 2B) and PAX8-SOX2 (Fig. 2C). Immunofluorescence conducted after induction of hair cell differentiation showed that cells derived from CP-iPSCs simultaneously expressed ATOH1 and POU4F3 (Fig. 3A), POU4F3 and MYO7A (Fig. 3B), and POU4F3 and Espin (Fig. 3C), the same as hair cells derived from C-iPSCs. Moreover, the total protein was extracted from hair cell-like cells derived from CP-iPSCs and immunoblotted for MYO7A. The results revealed the absence of the mutant (truncated) protein band (Fig. 4D); this demonstrated the successful correction of the *MYO7A* gene. We then identified F-actin and MYO7A double-labeled stereocilia-like protrusions in hair cell-like cells derived from CP-iPSCs (Fig. 4A). Scanning electron microscopy examination showed the recovery of the morphology of stereocilia-like protrusions (Fig. 4B), which was hard and straight. Several stereocilia appeared to stick together, similar to hair cell-like cells derived from normal iPSCs. In addition, hair cell-like cells derived from CP-iPSCs showed complete recovery of the uptake of FM1-43 (Fig. 5A). Moreover, electrophysiological detection also showed an outward K^+ current, inward rectifier K^+ current, and an inward Ca^{2+} current specific for hair cells (Fig. 5E). The I_{K1} and I_{Ca} recorded in hair cell-like cells derived from CP-iPSCs reached the same level as that in hair cell-like cells derived from C- and CF-iPSCs (Fig. 5F, 5G). These results indicated that the correction of mutations in the *MYO7A* gene in P-iPSCs led to the recovery of morphology and function of induced inner ear hair cell-like cells.

Discussion

The combination of iPSC technology with genome editing technology could offer a promising opportunity for treatment and cures for human inherited diseases, such as hereditary deafness. In the present study, we established three iPSC lines (P-iPSCs, CF-iPSCs, and C-iPSCs) from a hereditary deaf patient with compound heterozygous mutations in *MYO7A* (c.1184G>A and c.4118C>T), her father (expressing a *MYO7A* heterozygous mutation; c.1184G>A), and a normal donor. The c.4118C>T mutation site, which facilitated the identification of successful site correction by restriction digestion with the endonuclease *BstAP*I, was chosen for subsequent genetic correction. Therefore, iPSCs from the father (and not the mother) of the patient were used as the control for iPSCs derived from patients with a genetically corrected c.4118C>T mutation. All three iPSCs showed iPSC-like pluripotency, which indicated that the *MYO7A* mutations did not influence the induction and pluripotency of iPSCs. Cells derived from all three iPSCs presented the same characteristics when induced to differentiate into otic progenitors. This could be attributed to the restricted expression of the *MYO7A* gene in mature hair cells [30]; moreover, MYO7A is not required for the differentiation and function of otic progenitors.

Although the differentiation and function of otic progenitors derived from the three iPSCs showed no significant difference, the morphology of the stereocilia-like protrusions of hair cell-like cells induced from P-iPSCs differed from those of the protrusions in cells induced from CF-iPSCs and C-iPSCs. This was attributed to the double mutations in *MYO7A*. At the tip of stereocilia of the inner ear hair cells, MYO7A forms a ternary complex with harmonin b and cadherin 23 through its tail domain [31, 32]. This ternary complex forms the basis of the tip link and is bound to the F-actin bundles of the stereocilia through the motor domain of MYO7A [33]. Therefore, MYO7A plays a major role in the assembly of stereocilia into a bundled array and in maintaining rigidity during dynamic movements of the bundle [34]. Self et al. [14] reported that stereocilia formed normal rows of bundles with graded heights, which became progressively more disorganized in *Myo7a*^{816SB} and *Myo7a*^{6J} mutant mice. The *MYO7A*$^{Hdb/+}$ mutation led to the disorganization of stereociliary bundles [35]. A c.1184G>A mutation of *MYO7A* found in a consanguineous Iranian family was thought to alter the charge of the motor domain, thereby altering the local pH and structure and/or function of its motor domain [36]. The other c.41184C>T mutation of *MYO7A* directly creates a premature stop codon and thereby the removal of the last 842 residues of the protein, resulting in the non-integrity of the tail domain [37]. The MYO7A proteins expressed in the inner ear hair cell of this patient presented either the mutant motor domain or the truncated tail domain, which prevented anchoring of the tip link onto the stereocilia filled with F-actin bundles [38]. Therefore, the stereocilia on the hair cells of the patient with compound heterozygous mutations in *MYO7A* are not arrayed normally; in fact, the tip links between the stereocilia might not even exist. The tip of the hair stereocilia is the site at which MET occurs; moreover, tip-link filaments are believed to gate the MET channels [39–41]. The MET channels in the inner ear hair cells of deaf patients cannot be opened and closed normally, which might prevent the physical stimulus arising from sounds from transforming into currents, neurotransmitter release, and the formation of hearing sense, thereby causing deafness. In the present study, Western blot analysis revealed that the truncated MYO7A protein in cells induced from P-iPSCs was a result of the heterozygous nonsense c.4118C>T mutation in the ferm1 domain of one *MYO7A* locus. Therefore, it was inferred that neither of the MYO7A proteins translated from the allelic genes of the patient were normal and that the compound heterozygous mutations (localized in the motor domain of one MYO7A protein and in the ferm1 domain of another MYO7A protein, respectively) led to its dysfunction in shaping stereociliary bundles. The stereocilia-like protrusions in hair cell-like cells induced from CF-iPSCs was similar to that observed in cells induced from C-iPSCs, which indicated that only the MYO7A protein expressed from a normal heterozygous MYO7A locus was enough to maintain the normal morphology of the stereocilia-like protrusions. In addition, the rate of FM1-43-labeled P-iPSC-derived hair cell-like cells was much lower than that of hair cell-like cells derived from C- and CF-iPSCs. Some studies have shown that FM1-43 rapidly and specifically labels hair cells in the inner ear by entering the open mechanotransduction

(*Figure legend continued from previous page*.)
mutation); CP-iPSCs, genetically corrected induced pluripotent stem cells; DAPI, 4′,6-diamidino-2-phenylindole; I_{Ca}, inward Ca^{2+} current; I_{K1}, inward rectifier K^+ current; iPSC, induced pluripotent stem cell; ns, not significant; P-iPSCs, induced pluripotent stem cells from deaf patient with compound heterozygous *MYO7A* mutations (c.1184G>A and c.4118C>T).

channels [42]. Hair cells with *MYO7A* mutations that facilitate transduction but have all mechanotransduction channels closed at rest are not labeled with FM1-43 unless the bundles are stimulated by large excitatory stimuli [43]. Kros et al. [44] reported that MYO7A was required for normal gating of transducer channels. Mechanoelectrical transduction in the hair bundle induces an influx of K^+ and Ca^{2+} ions that depolarize hair cells [45]. MYO7A mutations might induce a decrease in mechanoelectrical transduction, thereby resulting in the absence of transducer current at rest, slow activation kinetics of the channel in hair cell-like cells derived from P-iPSCs, and a change in the concentration of K^+ and Ca^{2+}. Therefore, we concluded that the *MYO7A* compound heterozygous mutations led to mechanotransduction channel dysfunction and, consequently, to abnormal electrophysiological activity of hair cell-like cells derived from P-iPSCs.

In order to confirm that the phenotypic differences among hair cell-like cells derived from three different types of iPSCs were caused by *MYO7A* mutations and to restore the normal phenotype of hair cell-like cells derived from P-iPSCs, the *MYO7A* mutation was corrected using the CRISPR method. The parents of the patient were asymptomatic and displayed only one heterozygous mutation in the *MYO7A* gene; moreover, the cells induced from CF-iPSCs displayed the same normal phenotype as the cells induced from C-iPSCs. Therefore, we theorized that the correction of only one mutation site could be enough to restore the function of hair cells. In order to facilitate the identification of mutation site to be corrected by Western blotting, we selected the *MYO7A* c.4118C>T mutation in P-iPSCs to be genetically corrected using the CRISPR-Cas9 technology, thereby generating a new, corrected iPSC line (CP-iPSCs). The differentiation of CP-iPSCs into hair cell-like cells was then induced. Western blotting for MYO7A revealed the absence of truncations in the MYO7A protein in hair cell-like cells derived from CP-iPSCs; this indicated that genetic corrections of the R1373X mutation site resulted in normal expression of the MYO7A protein. In addition, stereocilia-like protrusions from the hair cell-like cells derived from CP-iPSCs recovered to the same organizational form as those from hair cell-like cells derived from C- and CF-iPSCs. In addition, FM1-43 uptake and the I_{K1} and I_{Ca} levels returned to normal in hair cell-like cells derived from CP-iPSCs (similar to that of hair cell-like cells derived from C- and CF-iPSCs), indicating that the MET channel had recovered. These results indicated that the correction of one mutation site in P-iPSCs was enough to recover the function of inner ear hair cell-like cells induced from P-iPSCs and that the phenotypic differences among hair cell-like cells derived from C-, CF-, and P-iPSCs were a result of *MYO7A* compound heterozygous mutations.

In the present study, we discovered that the stereocilia-like protrusions in hair cell-like cells induced from human iPSCs were atypical of the stereociliary bundles in the mammalian cochlea. Although stereocilia-like protrusions of hair cell-like cells differentiated from C-, CF- and CP-iPSCs appeared to be hard, straight, and stuck together, the obtained cilia were not typical stereociliary bundles, because they lacked certain structural hallmarks, such as a stair case pattern. We inferred that this induction method would need to be improved to promote the formation of stereociliary bundles in hair cell-like cells. The reorientation of stereociliary bundles occurs during normal embryonic development and regeneration of hair cells following acoustic trauma [46]. Differentiating stereociliary bundles establish asymmetric linkages with the extracellular matrix of the developing tectorial membrane in vivo. The growth of the tectorial membrane involves a progressive extension of the membrane across the surface of the sensory epithelium, which might exert traction forces through these asymmetric linkages, in turn pulling the bundles of hair cells into uniform alignment [46]. Additionally, Wnt signaling regulates the development of unidirectional stereociliary bundle orientation, and the lack of Wnts might result in nonstandard orientation of stereociliary bundles. As a result, standard links between induced stereocilia are very rare [47, 48]. Therefore, further studies must focus on identifying the mechanism by which the formation of typical stereociliary bundles is promoted by imitating the microenvironment of tectorial membrane and regulating the Wnt signaling during the induction of hair cell-like cells from human iPSCs.

The defective phenotype was a result of hereditary gene mutations, inner ear hair cell dysfunction, which is unlikely to be cured by drugs. Therefore, gene correction could be an ideal treatment method in the future. Hanna et al. [49] reported a classic gene therapy model using iPSCs, in which mice with humanized sickle cell anemia were rescued after transplantation with hematopoietic progenitors obtained in vitro from autologous iPSCs that had undergone correction of the human sickle hemoglobin allele by gene-specific targeting. Cells derived from iPSCs that are corrected genetically for therapeutic purposes appropriately bypass the paucity of sources. Therefore, these iPSCs can be induced repeatedly into the desired cell type, avoiding the anticipated immune rejection associated with allogeneic cell transplantation. In the present study, we developed hair cell-like cells with normal stereocilia-like protrusion structure and physiological activity from CP-iPSCs. Therefore, transplantation of these functionally recovered cells could be a promising therapy for deafness resulting from gene mutation. Nevertheless, several obstacles need to be overcome to transplant cells derived from iPSCs for hair cell regeneration. First, new reprogramming strategies for iPSCs should replace the use of oncogenic transcription factors (e.g., c-Myc) to eliminate the potential risk of tumorigenicity [50]. For example, nonintegrated vectors such as adenovirus vectors are used to avoid transgene integration [51], and the protein and micro-RNA methods are used to directly reprogram the somatic cells [52, 53]. Second, differentiation systems and cell sorting methods of greater efficiency should be developed to derive a clinically relevant number of purified otic progenitors or inner ear hair cells. Third, a systematic off-target analysis must be performed after gene correction to ensure that the genotypes of cells used in therapy are normal. Finally, the insertion and integration of cells into the auditory epithelium of the inner ear is a complicated task because of the hostile, high potassium environment of scala media [54] in the cochlea, and the robust junctional complexes between cells in the auditory epithelium [55]. Therefore, identifying a proper insertion method and drugs or reagents to transiently change the internal environment of auditory epithelium might facilitate the survival and integration of exogenously transplanted cells [56].

CONCLUSION

iPSCs were generated from a deaf patient with compound heterozygous *MYO7A* mutations (c.1184G>A and c.4118C>T), and one of *MYO7A* mutation sites (c.4118C>T) in the iPSCs was corrected using CRISPR/Cas9. The genetic correction of *MYO7A* mutation resulted in morphologic and functional recovery of hair cell-like cells derived from iPSCs. The current findings have confirmed

the hypothesis: MYO7A plays an important role in the assembly of stereocilia into stereociliary bundles. Therefore, our studies could provide further insight into the pathogenesis of sensorineural hearing loss and facilitate the development of therapeutic strategies against monogenic disease through the genetic repair of patient-specific iPSCs.

Acknowledgments

This study was supported by the grants from the National Basic Research Program of China (Grants 2012CB967902 and 2014CB541705), the National Development Program of Important Scientific Instruments (Grant 2013YQ030595), the Strategically Guiding Scientific Special Project from Chinese Academy of Sciences (Grant XDA04020202-23), the Opening Foundation of the State Key Laboratory of Space Medicine Fundamentals and Application (Grant SMFA12K02), the TZ-1 Application Program (Grant KYTZ01-0901-FB-003), and the Chinese National Science Foundation (Grant 81570932). We also thank Rui-Jian Zhu for help with karyotype analysis.

Author Contributions

Z.-H.T.: initial manuscript writing, experiment performance, data analysis and interpretation; J.-R.C., J.D., X.-D.Q., C.Z., J.-L.C., C.-C.W., and L.L.: experiment performance, data analysis and interpretation; J.Z., J.-Z.C., and T.-S.H.: collection and/or assembly of data; H.-S.S. and S.-K.Y.: electrophysiological recording; P.C. and M.-X.G.: conception and design, experimental design, project progression monitoring, data analysis and interpretation; J.-F.W.: conception and design, experimental design, project progression monitoring, data analysis and interpretation, final manuscript writing.

Disclosure of Potential Conflicts of Interest

The authors indicate no potential conflicts of interest.

References

1 Chen W, Jongkamonwiwat N, Abbas L et al. Restoration of auditory evoked responses by human ES-cell-derived otic progenitors. Nature 2012;490:278–282.

2 Ronaghi M, Nasr M, Ealy M et al. Inner ear hair cell-like cells from human embryonic stem cells. Stem Cells Dev 2014;23:1275–1284.

3 Takahashi K, Tanabe K, Ohnuki M et al. Induction of pluripotent stem cells from adult human fibroblasts by defined factors. Cell 2007; 131:861–872.

4 Zhou T, Benda C, Duzinger S et al. Generation of induced pluripotent stem cells from urine. J Am Soc Nephrol 2011;22:1221–1228.

5 Hanna J, Markoulaki S, Schorderet P et al. Direct reprogramming of terminally differentiated mature B lymphocytes to pluripotency. Cell 2008;133:250–264.

6 Brown ME, Rondon E, Rajesh D et al. Derivation of induced pluripotent stem cells from human peripheral blood T lymphocytes. PLoS One 2010;5:e11373.

7 Dimos JT, Rodolfa KT, Niakan KK et al. Induced pluripotent stem cells generated from patients with ALS can be differentiated into motor neurons. Science 2008;321:1218–1221.

8 Ebert AD, Yu J, Rose FF Jr et al. Induced pluripotent stem cells from a spinal muscular atrophy patient. Nature 2009;457:277–280.

9 Zwi-Dantsis L, Huber I, Habib M et al. Derivation and cardiomyocyte differentiation of induced pluripotent stem cells from heart failure patients. Eur Heart J 2013;34:1575–1586.

10 Teo AKK, Windmueller R, Johansson BB et al. Derivation of human induced pluripotent stem cells from patients with maturity onset diabetes of the young. J Biol Chem 2013;288: 5353–5356.

11 Liu XZ, Walsh J, Tamagawa Y et al. Autosomal dominant non-syndromic deafness caused by a mutation in the myosin VIIA gene. Nat Genet 1997;17:268–269.

12 Weil D, Küssel P, Blanchard S et al. The autosomal recessive isolated deafness, DFNB2, and the Usher 1B syndrome are allelic defects of the myosin-VIIA gene. Nat Genet 1997;16: 191–193.

13 Hasson T, Gillespie PG, Garcia JA et al. Unconventional myosins in inner-ear sensory epithelia. J Cell Biol 1997;137:1287–1307.

14 Self T, Mahony M, Fleming J et al. Shaker-1 mutations reveal roles for myosin VIIA in both development and function of cochlear hair cells. Development 1998;125:557–566.

15 Prosser HM, Rzadzinska AK, Steel KP et al. Mosaic complementation demonstrates a regulatory role for myosin VIIa in actin dynamics of stereocilia. Mol Cell Biol 2008;28: 1702–1712.

16 Li H, Liu H, Corrales CE et al. Correlation of Pax-2 expression with cell proliferation in the developing chicken inner ear. J Neurobiol 2004;60:61–70.

17 Hans S, Liu D, Westerfield M. Pax8 and Pax2a function synergistically in otic specification, downstream of the Foxi1 and Dlx3b transcription factors. Development 2004;131: 5091–5102.

18 Kiernan AE, Pelling AL, Leung KKH et al. Sox2 is required for sensory organ development in the mammalian inner ear. Nature 2005;434: 1031–1035.

19 Lawoko-Kerali G, Rivolta MN, Holley M. Expression of the transcription factors GATA3 and Pax2 during development of the mammalian inner ear. J Comp Neurol 2002;442: 378–391.

20 Brown ST, Wang J, Groves AK. Dlx gene expression during chick inner ear development. J Comp Neurol 2005;483:48–65.

21 Zheng W, Huang L, Wei ZB et al. The role of Six1 in mammalian auditory system development. Development 2003;130: 3989–4000.

22 Zou D, Silvius D, Fritzsch B et al. Eya1 and Six1 are essential for early steps of sensory neurogenesis in mammalian cranial placodes. Development 2004;131:5561–5572.

23 Zou D, Silvius D, Rodrigo-Blomqvist S et al. Eya1 regulates the growth of otic epithelium and interacts with Pax2 during the development of all sensory areas in the inner ear. Dev Biol 2006;298:430–441.

24 Chen P, Johnson JE, Zoghbi HY et al. The role of Math1 in inner ear development: Uncoupling the establishment of the sensory primordium from hair cell fate determination. Development 2002;129:2495–2505.

25 Cafaro J, Lee GS, Stone JS. Atoh1 expression defines activated progenitors and differentiating hair cells during avian hair cell regeneration. Dev Dyn 2007;236:156–170.

26 Bermingham NA, Hassan BA, Price SD et al. Math1: An essential gene for the generation of inner ear hair cells. Science 1999;284: 1837–1841.

27 Xiang M, Gan L, Li D et al. Essential role of POU-domain factor Brn-3c in auditory and vestibular hair cell development. Proc Natl Acad Sci USA 1997;94:9445–9450.

28 Elgoyhen AB, Johnson DS, Boulter J et al. α9: An acetylcholine receptor with novel pharmacological properties expressed in rat cochlear hair cells. Cell 1994;79: 705–715.

29 Bartles JR. Parallel actin bundles and their multiple actin-bundling proteins. Curr Opin Cell Biol 2000;12:72–78.

30 Hasson T, Heintzelman MB, Santos-Sacchi J et al. Expression in cochlea and retina of myosin VIIa, the gene product defective in Usher syndrome type 1B. Proc Natl Acad Sci USA 1995;92:9815–9819.

31 Boëda B, El-Amraoui A, Bahloul A et al. Myosin VIIa, harmonin and cadherin 23, three Usher I gene products that cooperate to shape the sensory hair cell bundle. EMBO J 2002;21: 6689–6699.

32 Bahloul A, Michel V, Hardelin JP et al. Cadherin-23, myosin VIIa and harmonin, encoded by Usher syndrome type I genes, form a ternary complex and interact with membrane phospholipids. Hum Mol Genet 2010;19: 3557–3565.

33 Heissler SM, Manstein DJ. Functional characterization of the human myosin-7a motor domain. Cell Mol Life Sci 2012;69:299–311.

34 Hasson T. Molecular motors: Sensing a function for myosin-VIIa. Curr Biol 1999;9: R838–R841.

35 Rhodes CR, Hertzano R, Fuchs H et al. A Myo7a mutation cosegregates with stereocilia defects and low-frequency hearing impairment. Mamm Genome 2004;15:686–697.

36 Hildebrand MS, Thorne NP, Bromhead CJ et al. Variable hearing impairment in a DFNB2

family with a novel MYO7A missense mutation. Clin Genet 2010;77:563–571.

37 Jaijo T, Aller E, Oltra S et al. Mutation profile of the MYO7A gene in Spanish patients with Usher syndrome type I. Hum Mutat 2006;27: 290–291.

38 Flock A, Bretscher A, Weber K. Immunohistochemical localization of several cytoskeletal proteins in inner ear sensory and supporting cells. Hear Res 1982;7:75–89.

39 Corey D. Sensory transduction in the ear. J Cell Sci 2003;116:1–3.

40 Gillespie PG, Walker RG. Molecular basis of mechanosensory transduction. Nature 2001; 413:194–202.

41 Hudspeth AJ. How hearing happens. Neuron 1997;19:947–950.

42 Meyers JR, MacDonald RB, Duggan A et al. Lighting up the senses: FM1-43 loading of sensory cells through nonselective ion channels. J Neurosci 2003;23:4054–4065.

43 Gale JE, Marcotti W, Kennedy HJ et al. FM1-43 dye behaves as a permeant blocker of the hair-cell mechanotransducer channel. J Neurosci 2001;21:7013–7025.

44 Kros CJ, Marcotti W, van Netten SM et al. Reduced climbing and increased slipping adaptation in cochlear hair cells of mice with Myo7a mutations. Nat Neurosci 2002;5:41–47.

45 Fettiplace R, Ricci AJ. Adaptation in auditory hair cells. Curr Opin Neurobiol 2003;13: 446–451.

46 Cotanche DA, Corwin JT. Stereociliary bundles reorient during hair cell development and regeneration in the chick cochlea. Hear Res 1991;52:379–402.

47 Dabdoub A, Donohue MJ, Brennan A et al. Wnt signaling mediates reorientation of outer hair cell stereociliary bundles in the mammalian cochlea. Development 2003;130: 2375–2384.

48 Qian D, Jones C, Rzadzinska A et al. Wnt5a functions in planar cell polarity regulation in mice. Dev Biol 2007;306:121–133.

49 Hanna J, Wernig M, Markoulaki S et al. Treatment of sickle cell anemia mouse model with iPS cells generated from autologous skin. Science 2007;318:1920–1923.

50 Jalving M, Schepers H. Induced pluripotent stem cells: Will they be safe? Curr Opin Mol Ther 2009;11:383–393.

51 Stadtfeld M, Nagaya M, Utikal J et al. Induced pluripotent stem cells generated without viral integration. Science 2008;322:945–949.

52 Zhou H, Wu S, Joo JY et al. Generation of induced pluripotent stem cells using recombinant proteins. Cell Stem Cell 2009; 4:381–384.

53 Warren L, Manos PD, Ahfeldt T et al. Highly efficient reprogramming to pluripotency and directed differentiation of human cells with synthetic modified mRNA. Cell Stem Cell 2010; 7:618–630.

54 Steel KP, Kros CJ. A genetic approach to understanding auditory function. Nat Genet 2001;27:143–149.

55 Nunes FD, Lopez LN, Lin HW et al. Distinct subdomain organization and molecular composition of a tight junction with adherens junction features. J Cell Sci 2006; 119:4819–4827.

56 Park YH, Wilson KF, Ueda Y et al. Conditioning the cochlea to facilitate survival and integration of exogenous cells into the auditory epithelium. Mol Ther 2014;22: 873–880.

57 Marcotti W, Géléoc GS, Lennan GW et al. Transient expression of an inwardly rectifying potassium conductance in developing inner and outer hair cells along the mouse cochlea. Pflugers Arch 1999;439: 113–122.

58 Chen W, Johnson SL, Marcotti W et al. Human fetal auditory stem cells can be expanded in vitro and differentiate into functional auditory neurons and hair cell-like cells. STEM CELLS 2009;27:1196–1204.

59 Platzer J, Engel J, Schrott-Fischer A et al. Congenital deafness and sinoatrial node dysfunction in mice lacking class D L-type Ca^{2+} channels. Cell 2000;102:89–97.

60 Marcotti W, Johnson SL, Rusch A et al. Sodium and calcium currents shape action potentials in immature mouse inner hair cells. J Physiol 2003;552:743–761.

See www.StemCellsTM.com for supporting information available online.

